China Ocean Eng., 2019, Vol. 33, No. 6, P. 637–648
DOI: 10.1007/s13344-019-0063-z, ISSN 0890-5487
http://www.chinaoceanengin.cn/ E-mail: coe@nhri.cn

Hydrodynamic Characteristics of Square Heaving Plates with Opening Under Forced Oscillation

CONG Long-fei, TENG Bin*

State Key Laboratory of Coastal and Offshore Engineering, Dalian University of Technology, Dalian 116024, China

Received May 13, 2019; revised July 16, 2019; accepted August 12, 2019

©2019 Chinese Ocean Engineering Society and Springer-Verlag GmbH Germany, part of Springer Nature

Abstract

The existence of the heaving plates can improve the heaving motion performance of an offshore structure significantly by providing both extra added mass and damping. In the current research, numerical investigation is carried out on the hydrodynamic characteristics of both isolated square heaving plate and double square heaving plates with opening by an immersed boundary-lattice Boltzmann method. The effects on hydrodynamic performance of plates due to Keulegan−Carpenter (*KC*) number, frequency number, opening ratio, opening distribution and spacing of plates are examined. It is found that the heaving plates with optimized opening ratio can provide additional damping compared with the plates without opening. Better hydrodynamic characteristics of double plates can be obtained with the increase of plate spacing.

Key words: immersed boundary-lattice Boltzmann method, square heaving plate, opening shape, opening ratio, opening distribution, plate spacing

Citation: Cong, L. F., Teng, B., 2019. Hydrodynamic characteristics of square heaving plates with opening under forced oscillation. China Ocean Eng., 33(6): 637–648, doi: 10.1007/s13344-019-0063-z

1 Introduction

Under the action of incident waves, a Spar type platform may experience large motion responses (Tao and Dray, 2008). Particular concern has been expressed by the engineers to the vertical component of such motion, i.e., the heaving motion. Large heaving motion may affect the operation condition of the platform, and such large motion may damage risers, drilling pipes and mooring lines. To minimize the heaving response, installing of heaving plates has been proven to be an effective way (Downie et al., 2000). Although the mass of the heaving plate itself is much smaller than that of the main part of the offshore structure, considerable added mass can be provided. It is well known that the heaving natural frequency of the offshore structure is mainly dependent on its inertia mass, added mass and waterline properties. With such added mass, the natural period of the offshore structure can be improved. On the other hand, with the help of the heaving plates, extra damping can be provided. Because of the relatively large submerged depth of the heaving plates, the radiation damping can be ignored and the viscous damping plays more important role. With such viscous damping, the heaving motion response of the platform can be further controlled.

In the past few decades, studies have been conducted to investigate the hydrodynamic characteristics of heaving plates both experimentally and numerically. Dependency of the added mass and the damping of the heaving plates on both the kinematic characteristics of the heaving motion, i.e., the amplitude and the frequency, and the geometric configurations of the heaving plates have been observed. Under high Reynolds number (*Re*) and *KC* number, Prislin et al. (1998) carried out hydrodynamic tests on arrays of square flat plates and compared the single plate result with that of multiple plates. The results showed that the interaction between multiple plates is weakened and can be ignored with the increase of plate spacing. The effect of configuration of heaving plates on heaving response was studied by Downie et al. (2000) experimentally and the results showed that the heaving responses of the platforms with the smaller and perforated plates were larger than those with larger and solid ones. Holmes et al. (2001) obtained the Morison coefficients for the heaving plates under different flow conditions by CFD methods. Ji et al. (2003) carried out forced oscillation tests on single plate and double plates. Drag coefficients and inertia coefficients versus *Re* and *KC* are obtained. To investigate the effect of large opening on the hydrodynamic performance of the heaving plate, solid and porous plates with large central opening are tested by Chua et al. (2005). Their results showed that the greater the perforation ratio was, the lower the value of the added mass

Foundation item: This study was financially supported by the National Natural Science Foundation of China (Grant Nos. 51490672 and 51879039).
*Corresponding author. E-mail: bteng@dlut.edu.cn

coefficient and the higher the value of the drag coefficient would be. Spacing effects on hydrodynamic characteristics of heaving plates are investigated by Tao et al. (2007). The results showed the existence of critical spacing depending on *KC* which is mostly beneficial in terms of maximizing the damping of the system, the added mass and damping coefficient are rather stable if the spacing is beyond that limit. Tao and Dray (2008) further carried out tests on hydrodynamic characteristics of the solid and porous plates. The model tests revealed that, at high *KC* number, solid plate produces more damping, while at very low *KC* number, the porous plate produces more damping. The effects of geometric details of the edge on the hydrodynamic performance of the heaving plates are studied by Shen et al. (2012) adopting CFD method and pretty good hydrodynamic performance has been obtained. Li et al. (2013) investigated the hydrodynamic coefficients of an isolated plate and multiple plates under forced oscillation by model tests. The effects of *KC* number, oscillation frequency, plate depth, thickness-to-width ratio, shape of the edge, perforation ratio, opening size and the spacing of the plates were analyzed in detail. Further, as the extension of the works by Thiagarajan and Troesch (1998) and Holmes et al. (2001), Yang et al. (2014) investigated the effect of in-plane current on the hydrodynamic characteristics of the heaving plate.

According to the mentioned works, there are many relevant works about the hydrodynamic characteristics of porous heaving plate. As pointed out by Chua et al. (2005), the heaving plates always have perforated holes due to the need of running vertical risers and the geometric characteristic of the holes plays an important role on their hydrodynamic characteristics. In most works, small openings are uniformly distributed on the heaving plate. Actually, too many small openings may have negative effect on the strength of the structures because of the stress concentration, during both production stage and service stage of the plates. By considering this fact, fewer but larger openings may be more feasible in practice. In the present research, the hydrodynamic characteristics of both isolated square heaving plate and double square heaving plates with concentrated opening are investigated by an immersed boundary-lattice Boltzmann method (IB-LBM). The effects of *KC* number, frequency number and the spacing on the hydrodynamic characteristics of the plates are examined. As the key factors to affect the hydrodynamic characteristics of the plates, the size and the distribution of the openings are also discussed.

2 Mathematical formulations and numerical method

In the current research, a Cartesian coordinate system is adopted. The Navier−Stokes (N−S) equations for incompressible viscous fluid is applied to describe the fluid flow, which can be written as

$$\boldsymbol{u}_t + (\boldsymbol{u}\cdot\nabla)\boldsymbol{u} = -\frac{1}{\rho}\nabla p + \nu\nabla^2\boldsymbol{u} + \boldsymbol{f}_{\mathrm{ib}},$$
$$\nabla\cdot\boldsymbol{u} = 0, \tag{1}$$

where $\boldsymbol{u}$ is the velocity vector of the fluid flow, ρ the density of the fluid, p and ν the pressure and the kinetic viscosity of the fluid respectively. $\boldsymbol{f}_{\mathrm{ib}}$ is the body force caused by the immersed boundary of the plate.

To investigate the hydrodynamic characteristics of the heaving plates, infinitely thin square plates are adopted as the model and are forced to oscillate periodically. The schematic diagram of the heaving plates and the geometric characteristics of the plates are shown in Fig. 1 and Fig. 2 respectively. The displacement of the plates follows

$$Z(t) = A\cos(\omega t), \tag{2}$$

where A is the amplitude of the oscillation, and ω is the angular frequency of the oscillation. The velocity of the plates can be written as:

$$U_z(t) = \frac{\mathrm{d}Z(t)}{\mathrm{d}t} = -\omega A\sin(\omega t) = -U_{\max}\sin(\omega t), \tag{3}$$

where $U_{\max}$ is the maximum velocity during oscillation. The oscillation motion can be characterized by two dimensionless parameters, Keulegan−Carpenter number *KC* and the frequency number β, respectively. These parameters are defined as:

$$KC = \frac{2\pi A}{D} = \frac{U_{\max}T}{D},\ \beta = \frac{D^2}{\nu T}, \tag{4}$$

where D is the width of the plate and $T=2\pi/\omega$ is the period of the oscillation motion. The Reynolds number for the oscillation motion is defined as:

$$Re = \frac{U_{\max}D}{\nu} = (KC)\beta, \tag{5}$$

and the heaving force coefficient is calculated as:

$$C_z = \frac{F_z}{\frac{1}{2}\rho U_{\mathrm{ref}}^2 S_{\mathrm{ref}}}, \tag{6}$$

where F_z is the force component acting on the plate in the z direction. The calculation of such force will be explained in the following part.

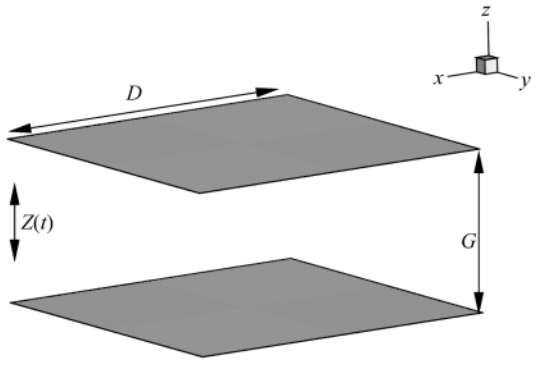

Fig. 1. Schematic diagram of the heaving plates.

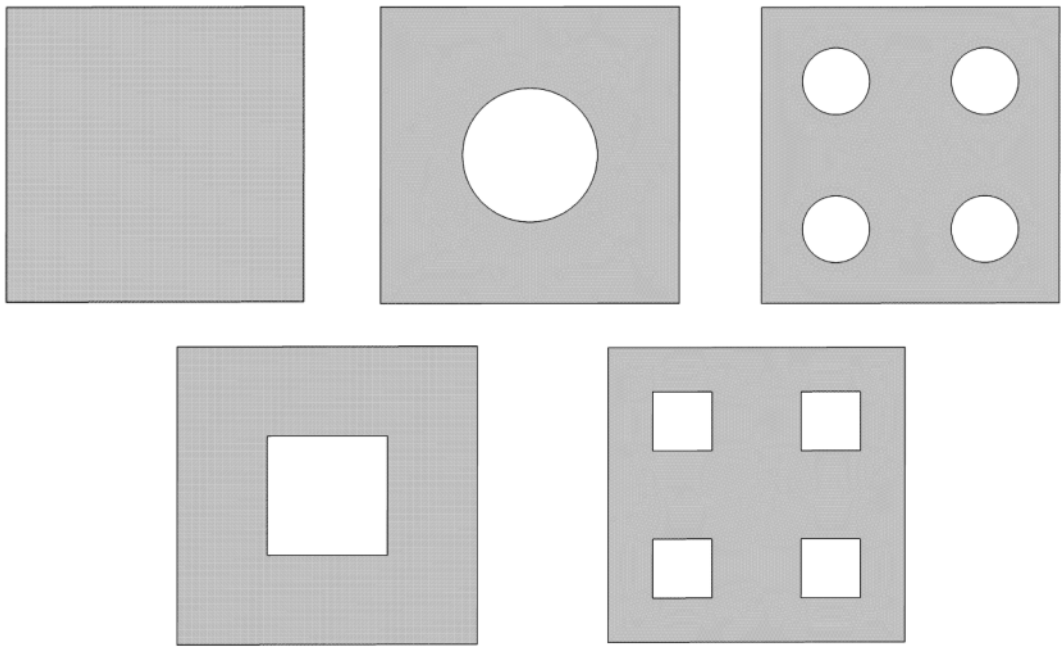

Fig. 2. Geometric characteristics of the plates.

The N−S equations can be solved by finite volume, finite difference or finite element based incompressible N−S solvers. For most existing codes based on the mentioned numerical model, the macroscopic equations for conservative variables, i.e., mass and momentum, are solved directly. In consideration of the computation cost, the pressure and velocity of the fluid are often solved in a segregate manner. To enforce the incompressibility of the fluid, a pressure-based velocity correction algorithm, such as SIMPLE series method (Patankar and Spalding, 1972) and projection method (Chorin, 1967), is used to achieve their coupling. For large scale numerical simulation, especially in 3D cases, because of the global characteristics of the pressure equation, the resulting large scale sparse linear system will take considerable computer resource to converge.

Compared with the traditional model, Lattice Boltzmann method (LBM) models the fluid as fictive particles and treats the incompressible flow as a weakly compressible one by forcing the local Mach number $Ma<<1$ to control the compressibility. The pressure of the fluid flow relates to its density in an explicit manner, such treatment avoids the process to get the pressure implicitly and improve the efficiency of the flow solver considerably. Further, the LBM equations are solved by adopting local collision-streaming operations, such property is attractive for parallelization. In the current research, considering its computational efficiency, LBM is used to solve the N−S equations. The nineteen-velocity model in three dimensions (D3Q19) together with multiple-relaxation-time (MRT) collision model (Lallemand and Luo, 2000) is adopted for its better numerical stability.

To achieve the no-slip boundary condition on the surface of the plates, immersed boundary method (IBM) is adopted in this study. Compared with the numerical model based on body-fitted grid, during the motion of solid body immersed in the fluid domain, only static grid is needed and the time-consuming re-meshing or mesh moving process is avoided, which further improves the accuracy and the efficiency of the flow solver. To consider the effect of solid boundary on the fluid flow, a body force $\boldsymbol{f}_{\mathrm{ib}}$ is added to the right hand side of the momentum part of N−S equations, as shown in Eq. (1). The body force relates to the interaction force between the plate and the fluid flow as:

$$\begin{aligned}
&\boldsymbol{f}_{\mathrm{ib}}(\boldsymbol{x},t) = -\sum_{n=1}^{N_{\mathrm{ib}}} D_h(\boldsymbol{x}-\boldsymbol{X}_{\mathrm{ib}}^n)\boldsymbol{F}_{\mathrm{ib}}(\boldsymbol{X}_{\mathrm{ib}}^n,t)\mathrm{d}s_n;\\
&D_h(\boldsymbol{x}) = \frac{1}{h^3}\Delta\left(\frac{x_1}{h}\right)\Delta\left(\frac{x_2}{h}\right)\Delta\left(\frac{x_3}{h}\right);\\
&\Delta(\cdot) = \begin{cases}
\dfrac{1}{8}(3-2|\cdot|+\sqrt{1+4|\cdot|-4|\cdot|^2}), & |\cdot|<1\\
\dfrac{1}{8}(5-2|\cdot|-\sqrt{-7+12|\cdot|-4|\cdot|^2}), & 1\leqslant|\cdot|<2\\
0, & 2\leqslant|\cdot|
\end{cases}
\end{aligned} \tag{7}$$

where N_{ib} is the number of panel nodes on the surface of the plate, $\boldsymbol{X}_{\mathrm{ib}}$ is the position vector of the panel node, ds is related to the area of the panel and h is the size of the local uniform grid. To achieve the velocity interpolation from LB grid to IB grid and force spreading from IB grid to LB grid, $D_h(\boldsymbol{x})$, the 3D smoothed delta function, is adopted and $\Delta(\cdot)$ is the 1D kernel function to construct $D_h(\boldsymbol{x})$. To obtain $\boldsymbol{F}_{\mathrm{ib}}$, direct forcing method is used. The details about such term can be seen in Feng and Michaelides (2005) and will not be discussed in detail hereinafter. The hydrodynamic force on

the plate can be obtained as:

$$\boldsymbol{F}=\sum_{n=1}^{N_{\mathrm{ib}}}\boldsymbol{F}_{\mathrm{ib}}(\boldsymbol{X}_{\mathrm{ib}}^{n},t)\mathrm{d}s_{n}. \tag{8}$$

With such body force, the LBM equation with MRT collision model can be written as:

$$\begin{aligned}
&q_{\alpha}(\boldsymbol{x}+\boldsymbol{e}_{\alpha}\delta t,t_n+\delta t)-q_{\alpha}(\boldsymbol{x},t_n)=-\boldsymbol{M}^{-1}\cdot\boldsymbol{S}\cdot\boldsymbol{M}\cdot\boldsymbol{Q}\big|_{\alpha}+F_{\alpha}\delta t,\\
&\boldsymbol{Q}=\left[q_0(\boldsymbol{x},t_n)-q_0^{\mathrm{eq}}(\boldsymbol{x},t_n),q_1(\boldsymbol{x},t_n)-q_1^{\mathrm{eq}}(\boldsymbol{x},t_n),...\right]^{\mathrm{T}},\\
&q_{\alpha}^{\mathrm{eq}}=\rho\omega_{\alpha}\left[1+\frac{\boldsymbol{e}_{\alpha}\cdot\boldsymbol{u}}{c_{\mathrm{s}}^2}+\frac{(\boldsymbol{e}_{\alpha}\cdot\boldsymbol{u})^2}{2c_{\mathrm{s}}^4}-\frac{\boldsymbol{u}\cdot\boldsymbol{u}}{2c_{\mathrm{s}}^2}\right],\\
&F_{\alpha}=\tilde{F}_{\alpha}-\frac{1}{2}\boldsymbol{M}^{-1}\cdot\boldsymbol{S}\cdot\boldsymbol{M}\cdot\tilde{\boldsymbol{F}}\big|_{\alpha},\ \tilde{\boldsymbol{F}}=\left[\tilde{F}_0,\tilde{F}_1,...\right]^{\mathrm{T}},\\
&\tilde{F}_{\alpha}=\omega_{\alpha}\rho\left(\frac{\boldsymbol{e}_{\alpha}-\boldsymbol{u}}{c_{\mathrm{s}}^2}+\frac{\boldsymbol{e}_{\alpha}\cdot\boldsymbol{u}}{c_{\mathrm{s}}^4}\boldsymbol{e}_{\alpha}\right)\cdot\boldsymbol{f}_{\mathrm{ib}},\ c_{\mathrm{s}}=\frac{h}{\sqrt{3}\delta t},\\
&\rho=\sum_{\alpha}q_{\alpha},\rho\boldsymbol{u}=\sum_{\alpha}\boldsymbol{e}_{\alpha}q_{\alpha}+\frac{1}{2}\rho\boldsymbol{f}_{\mathrm{ib}}\delta t,\ p=(\rho-\rho_0)c_{\mathrm{s}}^2,
\end{aligned} \tag{9}$$

where q_{α} and q_{α}^{eq} (α=1−19) are the distribution function and the equilibrium distribution function respectively, e_{α}(α=1−19) the discrete velocity vector and c_{s} the local sound velocity (Chen and Doolen, 1998). F_{α} (α=1−19) is the forcing term to consider the effect of body force (Guo et al., 2002). $\boldsymbol{M}$ is the transform matrix which maps the distribution function and the forcing term to the moment space and $\boldsymbol{S}$ is a diagonal matrix consisting of different relaxation rates (d'Humières, 2002). In the definition of p, ρ_0 is the undisturbed density of the fluid.

In the current research, local high resolution solution is obtained by adopting multi-grid technique. The local refinement method (Rohde et al., 2006) is used to achieve better conservation characteristics and independence on the collision model of LBM. In the current simulation for heaving plates, three levels of grid are adopted and the finest grid spacing h is D/80. The computational domain is set as 20D in the x, y and z directions. On all the domain boundaries, Dirichlet conditions are forced for the velocity and pressure of the fluid flow, where the velocity is set as 0 and the pressure is set to the undisturbed value. The reliability of the grid setting is tested in the appendix.

In the present study, direct numerical simulation (DNS) is carried out adopting LBM as the flow solver and IBM to consider the effect of solid boundary. It has been shown that LBM is an explicit flow solver, such explicit characteristic leads stability issues with the increase of Re and the way to remedy the issues is to increase the resolution or to adopt suitable turbulence model.

On one hand, for most turbulence models, empirical coefficients are introduced to close the system, leading to additional error during the simulation. On the other hand, for turbulence simulation, considerably large CPU resource must be paid to get the statistical properties of the flow fields. Such computer resource requirement is beyond what we have.

Further, the present version of the LBM code is based on the static multi-block local refinement method with OpenMP to achieve the parallel computation. With such model, the unchanged refinement region is formed around the possible path of the plate and such low level refinement model leads to too much CPU memory cost with the increase of refinement level, which is also beyond what we have. Actually, large eddy simulation (LES) with adaptive mesh refinement (AMR) is attractive to improve the performance of the solver and the AMR module and LES module in our code are still under development.

It should also be pointed out that, for fluid flow in the laminar region, its characteristics are much obvious and distinct than that for fluid flow in turbulence region. Although the detailed structure of the flow field in laminar region is much different from that in turbulence region, much similarity is shared in their large scale behaviors. With these facts, in the current research, only simulations about fluid flow with relatively low Re of $O(10^2)$ are carried out. Although the Re in the current research is much lower than that in practical engineering, we believe that the basic characteristics of the fluid flow are well captured.

In the current research, the λ_2 criterion (Jeong and Hussain, 1995) is used to identify the three dimensional vortical structures.

3 Validation

To validate the present IB-LBM model, calculations are carried out for the steady problem for flow caused by a stationary circular disk in normal incident flow and the unsteady problem for flow caused by an oscillating circular disk without incoming flow.

Firstly, following Shenoy and Kleinstreuer (2008), a circular disk with diameter D and thickness 0.1D is adopted, and the computational domain is set as 16D, 16D and 17D in the x, y and z directions respectively. The center of the disk is located 5D from the inflow boundary. A free stream velocity (0, 0, U_{s}) and undisturbed density are forced on all the boundaries. Three levels of grid are adopted for the local high resolution simulation and the finest grid is h=D/80. The surface of the disk is discretized into unstructured triangle elements and the scale of the element is comparable with the local grid spacing. The surface grid structure of the disk is shown in Fig. 3. It should be noticed that, adopting uniform grid in all three directions in LBM, the current resolution near the disk is much higher than that used by Shenoy and Kleinstreuer (2008).

Comparison of the drag coefficients is made between the results obtained by current IB-LBM model, finite volume (FV) based model, i.e., CFX in Shenoy and Kleinstreuer (2008) and model test (Roos and Willmarth, 1971), as shown in Fig. 4. In this case, Re_{s} denotes the Reynolds number based on the free stream velocity and the diameter of the disk.

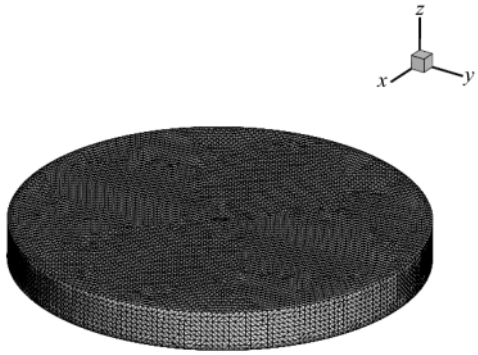

Fig. 3. Surface grid structure of the stationary circular disk.

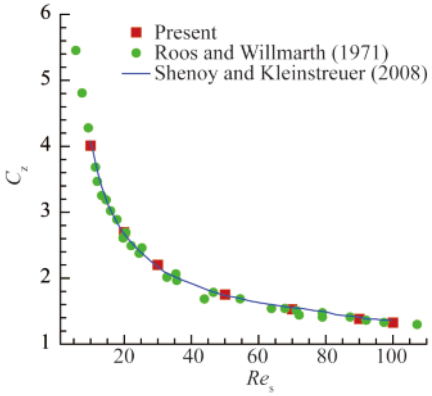

Fig. 4. Comparison of C_z between present results and previous ones for the steady flow normal to a stationary circular disk.

As observed by Shenoy and Kleinstreuer (2008), in the Reynolds number region considered here (i.e. $Re_s \leqslant 100$), the flow is steady and axisymmetric. In this case, the free stream velocity U_s is adopted as the reference velocity and the surface area facing the flow $\pi D^2/4$ is adopted as the reference area. Good agreement has been obtained between the current results and previous ones, both by numerical method (Shenoy and Kleinstreuer, 2008) and experimental method (Roos and Willmarth, 1971).

To make a further validation on the present IB-LBM model for simulation about unsteady flow caused by moving boundary. The unsteady flow caused by an oscillating circular disk is simulated (Tian et al., 2017). In this case, the disk is forced to oscillate periodically along its axis without incoming flow. The computational domain is set as $20D$ in the x, y and z directions. On the far field boundary, Dirichlet conditions are forced for the velocity and pressure of the fluid flow, where the velocity is set as 0 and the pressure is set to the undisturbed value. Five levels of grid are adopted, the finest grid spacing and time increment are $h=D/160$ and $\delta t=T/8000$ respectivily. The aspect ratio of the disk is set as 0.1. As observed by Tian et al. (2017), with Re ranging from 50 to 800 and KC ranging from 1 to 24, there are at least five flow regions, namely, axisymmetric flow region (AS), planar symmetric flow region in the low-KC region (PSL), azimuthally rotating flow region in the low-KC region (ARL), planar symmetric flow region in the high-KC region (PSH) and azimuthally rotating flow region in the high-KC region (ARH). With the relatively low KC and Re adopted in the present research, two typical cases with low KC and low Re, i.e., KC=2.57, Re=200 in AS region and KC=2.57, Re=411 in PSL region, are selected to make the validation. The time histories of the force coefficients are shown in Fig. 5 and the flow fields with the disks at their lowermost positions are shown in Fig. 6. It should be mentioned that, in the present study, the disks are forced to oscillate from their uppermost positions while Tian et al. (2017) forced the disks to oscillate from their equilibrium positions. The force coefficients have been corrected to consider such phase difference. Further, for horizontal forces, redirection is made to make C_Y=0. From Fig. 5a, no horizontal force can be observed with KC=2.57 and Re=200, indicating that the no symmetry breaking is formed with such parameters. As shown in Fig. 6a, in this case, the flow field shows obvious axisymmetric characteristics. With Re increase to 411, symmetry breaking can be observed and the disk experiences horizontal force during the oscillation. Comparison between present results and previous results by Tian et al. (2017) is made and good agreement has been obtained as shown in Fig. 5b. As shown in Fig. 6b, in the PSL region, the planar symmetric pattern, rather than the axisymmetric pattern can be observed around the disk. Such characteristic is consistent with that observed by Tian et al.

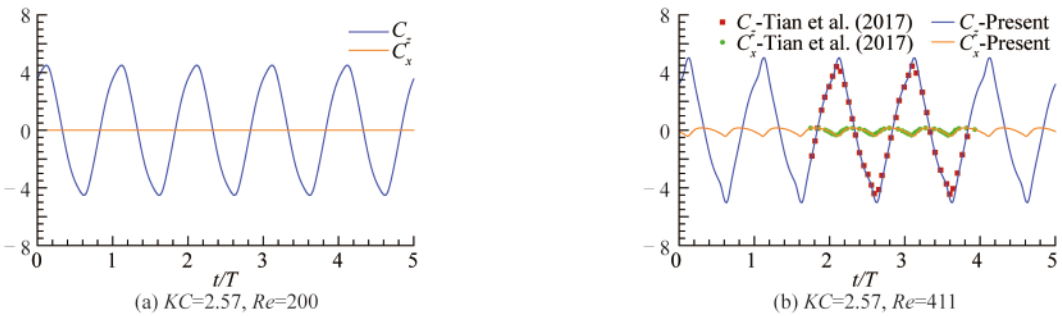

Fig. 5. Time histories of C_x and C_z for an oscillating circular disk.

(a) KC=2.57, Re=200 (b) KC=2.57, Re=411

Fig. 6. Flow fields for oscillating circular disks. The vortical structures around the disks are identified by λ_2 criterion and the iso-surfaces of $\lambda_2=-10f^2$ are shown. $f=1/T$ is the oscillating frequency.

(2017). According to these cases, the reliability of the present IB-LBM model is validated.

4 Results and discussions

In this section, the hydrodynamic characteristics of the heaving plates shown in Fig. 2 are investigated. The effects of KC number, frequency number, the size and the distribution of the opening and the spacing of the plates are examined. In the current research, three KC numbers, KC=0.50, 0.75, 1.00, and three frequency numbers, β=133, 200, 400, are adopted. The opening ratio of the plate is defined as S_{opening}/S_0, where S_{opening} denotes the area of opening and $S_0=D^2$ denotes the area of the plate without opening. Four types of opening, as shown in Fig. 2, are tested in the current research to consider the effects of opening shape and opening distribution on the hydrodynamic characteristics of the plates. Isolated plate and double plates with G/D=0.50, 0.75 and 1.00 are tested to consider the spacing effect.

In the current research, added mass coefficients and damping coefficients are adopted to describe the hydrodynamic characteristics of the plates. Consistent with the linear potential theory, the linear component of the hydrodynamic force on the plate, i.e., the heaving frequency component of the force, is considered and it can be expressed as:

$$F_z^{\text{linear}}(t)=\text{Re}[e^{-\text{i}\omega t}\tilde{Z}(\omega)(\omega^2 A_{33}+\text{i}\omega B_{33})], \quad (10)$$

where $\tilde{Z}(\omega)$ is the displacement of the plate in frequency domain.

4.1 Isolated plate

Firstly, the hydrodynamic characteristics of isolated heaving plates are investigated. As shown in Fig. 2, the square plates with single opening and four openings are adopted. The shape of the opening is either circle or square. To consider the effect of KC, β is fixed as 200 and to consider the effect of β, KC is fixed as 0.75.

4.1.1 *Added mass coefficient*

The added mass coefficients are shown in Figs. 7−10. From Figs. 7 and 8, it can be seen that for the isolated heaving plate, the added mass coefficients are almost identical and are not sensitive to the shape of the opening. With the increase of the opening ratio, the added mass decreases and it is more sensitive to the opening ratio when the opening ratio is small. The added mass increases with the increase of KC. When the opening ratio is small, the added mass nearly increases with KC linearly. Li et al. (2013) tested the plates with the opening ratio up to 0.1 and has observed linear de-

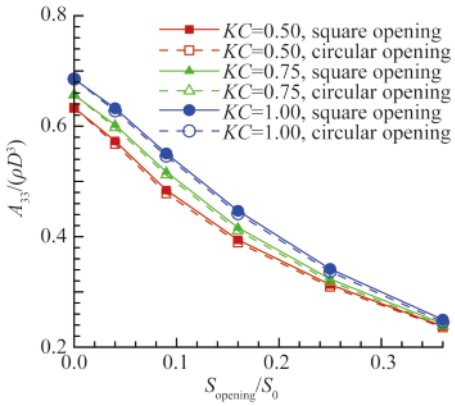

Fig. 7. Added mass coefficients of heaving plates with single opening and β=200.

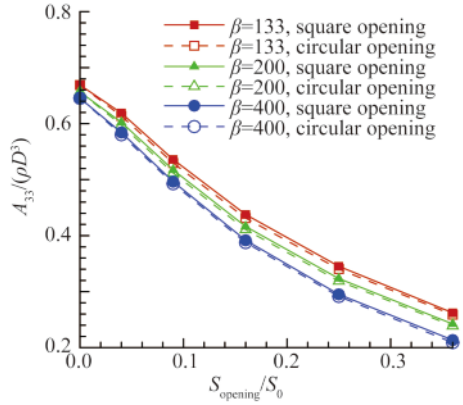

Fig. 8. Added mass coefficients of heaving plates with single opening and KC=0.75.

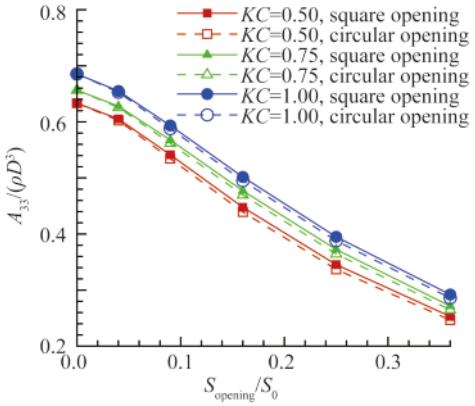

Fig. 9. Added mass coefficients of heaving plates with four openings and β=200.

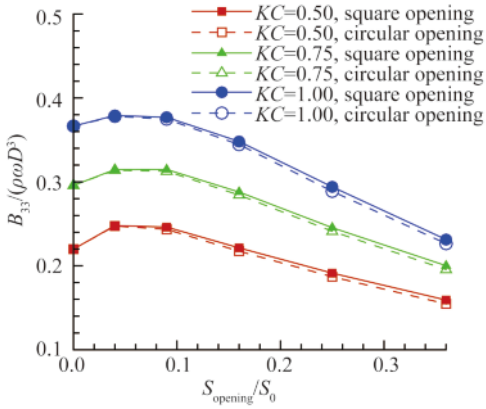

Fig. 11. Damping coefficients of heaving plates with single opening and β=200.

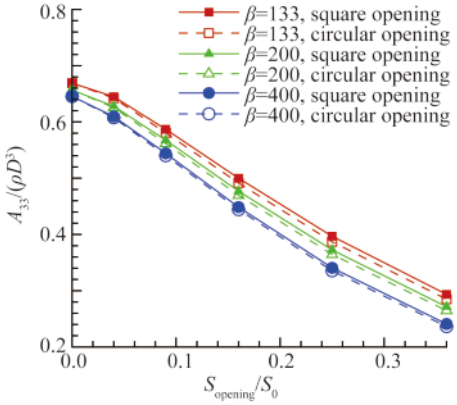

Fig. 10. Added mass coefficients of heaving plates with four openings and *KC*=0.75.

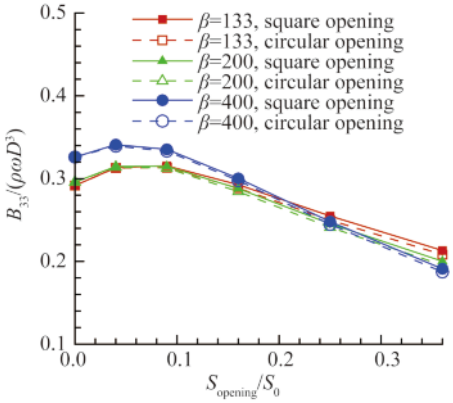

Fig. 12. Damping coefficients of heaving plates with single opening and *KC*=0.75.

pendency of the added mass on *KC*, which is consistent with the present results. With the increase of frequency number, the added mass decreases and such dependency is stronger when the opening ratio is large.

Figs. 9 and 10 show the added mass of the isolated plate with four openings. Similar to the plate with single opening, no obvious dependency of the added mass on the shape of the opening can be observed. Comparing the plate with single opening, we can see that the added mass of the plate with four openings is larger.

4.1.2 *Damping coefficient*

Figs. 11 and 12 show the damping coefficients of the isolated plate with single opening. It can be seen that the damping coefficients increase with *KC* over a wide range of opening ratio. When the opening ratio is small, the damping coefficients increase with frequency number, while the damping coefficients decrease with frequency number when larger opening ratio is adopted. For certain *KC* and frequency number, the damping coefficient firstly increases with opening ratio, when the opening ratio continues to increase from an optimized value around 0.1, the damping coefficient decreases. This phenomenon indicates that suitable opening of the plate has positive effect on the damping characteristics of the heaving plate, while too large opening has negative effect. Similar to the added mass coefficients, the damping coefficients show basically no dependency on the shape of the opening.

The effects of the opening distribution on the damping of the plates are further investigated and the results are shown in Figs. 13 and 14. The overall tendency is identical to that of the isolated plate with single opening. The damping coefficients firstly increase with the opening ratio, after reaching the peak value, further increase of the opening ratio has negative effect on the damping characteristics of the plate. Such phenomenon has also been observed by Wu et al. (2009).

4.2 Double plates

For Spar type platform, multiple heaving plates are often adopted to improve the hydrodynamic characteristics. To investigate the plate spacing effect on the hydrodynamic characteristics of multiple heaving plates, double plates with different spacings are adopted. In this section, only plates with circular opening are tested, *KC* is fixed as 0.75 and β is fixed as 200.

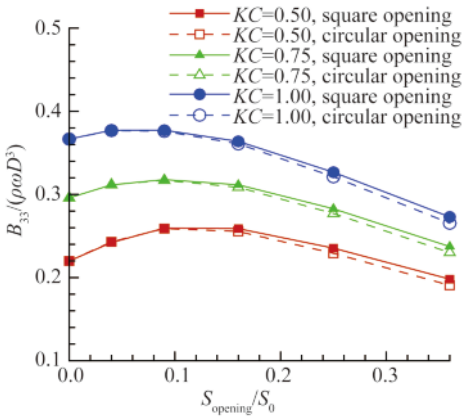

Fig. 13. Damping coefficients of heaving plates with four openings and β=200.

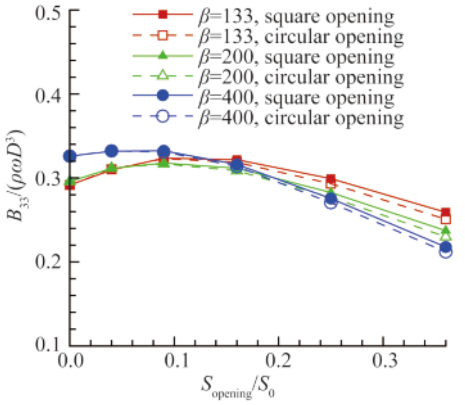

Fig. 14. Damping coefficients of heaving plates with four openings and KC=0.75.

4.2.1 *Added mass coefficient*

Figs. 15 and 16 show the added mass coefficients of the plates with different spacing and distribution of the openings. To simplify the problem, two identical plates are adopted and the averaged coefficients are presented for comparison. As shown in Fig. 15, it can be observed that the added mass coefficient increases with G/D. Although the total added mass of the double plates is larger, the added mass provided by each plate is smaller than that of the isolated plate. The added mass is more sensitive to the plate spacing when the opening ratio is small. When the opening ratio increases, such dependency is weakened. Similar tendency of the added mass can be obtained when four openings are adopted. Compared with the case with single opening, larger added mass can be provided adopting such opening distribution.

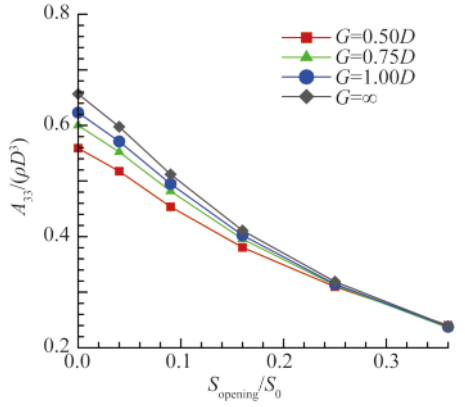

Fig. 15. Added mass coefficients of double heaving plates with single opening and KC=0.75, β=200.

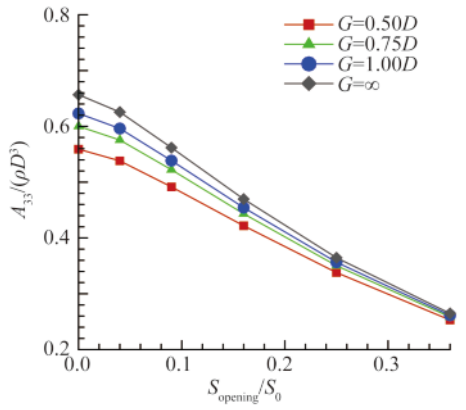

Fig. 16. Added mass coefficients of double heaving plates with four openings and KC=0.75, β=200.

In fact, based on a heaving cylinder with two attached circular disks, the dependency of hydrodynamic properties on span-wise length has been investigated by Tao et al. (2007). Their results reveal that the relative spacing of the plates is an important factor to influence the hydrodynamic characteristics. Beyond the critical spacing for a definite plate, the hydrodynamic coefficients are independent on the relative spacing. Li et al. (2013) obtained similar conclusion in their experimental study. The current results are consistent with the previous ones. Moreover, from the current results, phenomenon can be observed that the critical value decreases with the increase of opening ratio.

4.2.2 *Damping coefficient*

Figs. 17 and 18 show the averaged damping coefficients of the double plates with single opening and four openings. The damping increases with plate spacing. Similar to the isolated plate, the optimized opening ratio exists in the sense of damping generation. For plates with four openings, the damping is larger than that of plates with single opening.

4.3 Flow visualisations

As pointed out by Tao et al. (2007), the damping of a heaving plate has close relationship with the vortex shedding around the plate. It is obvious that such vortex shedding depends on the motion style, the opening ratio and opening shape of the plate. To make a deep understanding of the mechanism of the damping generation, flow fields of the heaving plates are investigated in this section.

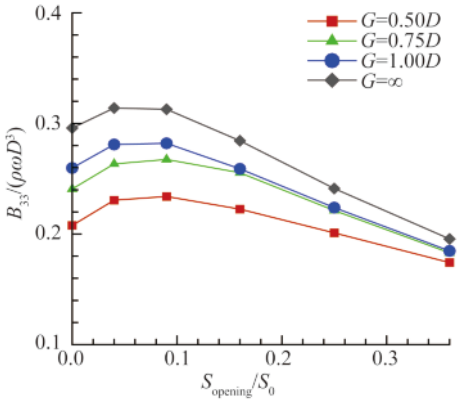

Fig. 17. Damping coefficients of double heaving plates with single opening and KC=0.75, β=200.

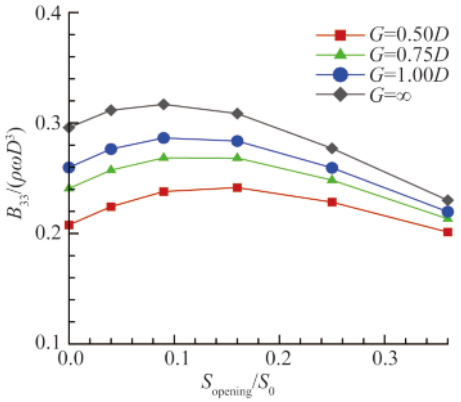

Fig. 18. Damping coefficients of double heaving plates with four openings and KC=0.75, β=200.

According to the results presented in the previous sections, compared with the other factors affecting the hydrodynamic characteristics of the heaving plate, the characteristics of the opening and the spacing of the plates play more important roles. In this section, KC is fixed as 0.75 and β is fixed as 200.

Firstly, the flow field of an isolated plate with opening ratio 0.16 is presented. Fig. 19 shows the vortex fields of the plates with different opening shape. In this section, the plates are at the position with the maximum negative heaving velocity.

Comparing the flow fields of the plates with circular and square openings, we can see that the vortex distributions are similar, strong vortex shedding can be observed around the sharp edge of the plate and around the opening. The vortical structures around the sharp edge of the plates are basically identical to each other. Vortex shedding is mainly generated around the edge rather than the corner of the plate at this relatively low Re. Similar vortex structure can be observed around the edge of the opening. For different opening shapes, although the 3D vortical structure shows difference around the corner of the opening, no obvious difference can be observed for the main vortical structure on the

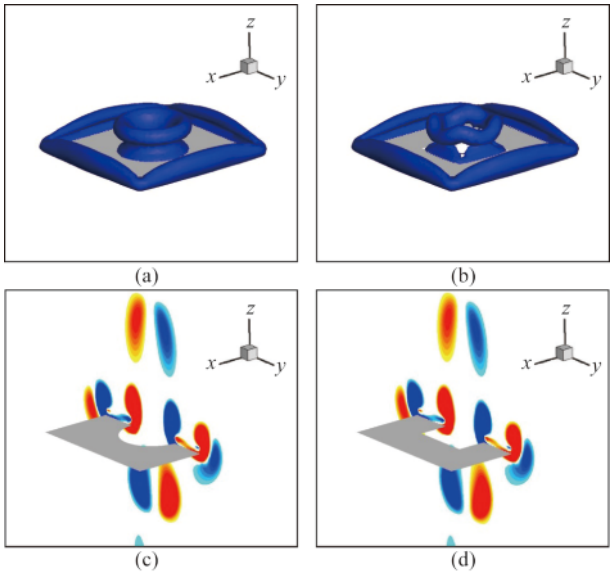

Fig. 19. Flow visualisations of the heaving plates with (a, c) single circular opening and (b, d) single square opening. (a, b) present the 3D vortical structure around the plates identified by λ_2 criterion, where the iso-surfaces of $\lambda_2=-50f^2$ are shown. (c, d) show the ω_x contours from $-5f$ (blue) to $+5f$ (red). $f=1/T$ is the heaving frequency.

centre plane of the opening, as shown in Figs. 19c and 19d. Because of such similarity, the hydrodynamic characteristics show no obvious dependency on the opening shape. Such independency indicates that the vortex shedding around the edge, rather than the corner of the plate, makes the main contribution to the generation of damping. With the effect of opening distribution on the flow fields, the flow fields of plates with four openings are shown in Fig. 20. Similar to the plate with single opening, the vortical structure shows no obvious difference between the plates with four circular openings and four square openings. Compared with that of the plate with single opening, the flow field is different. Around each opening, obvious vortex shedding can be observed. As pointed out by Tao et al. (2007), the damping performance of a plate has close relationship with the vortex shedding from it. Based on such observation, larger damping of the plate with four openings can be explained by this stronger vortex shedding.

Vortical structures of plates with different opening ratios are shown in Fig. 21. As mentioned previously, the shape effect is limited. In Fig. 21, only the flow fields of the plates with circular opening are shown.

Although the geometric configuration adopted in this research is significantly different from that used by Tao and Thiagarajan (2003) and Yang et al. (2014), the vortical fields shown in Fig. 21 appear to be in the interactive flow regime. Symmetric vortex pattern is generated over one heaving period. As shown in Fig. 21, the newly generated vortex interacts with the previous one. Further, it can be observed that with the increase of the opening ratio, weaker vortex shedding can be observed around the edge of the

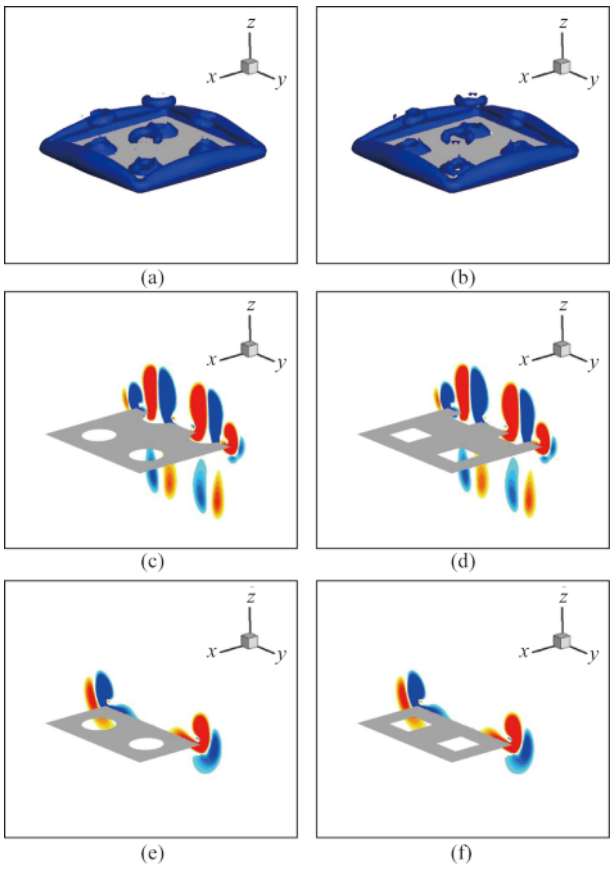

Fig. 20. Flow visualisations of the heaving plates with (a, c, e) four circular openings and (b, d, f) four square openings. (a, b) present the 3D vortical structure around the plates identified by λ_2 criterion, where the iso-surfaces of λ_2=−50f^2 are shown. (c, d, e, f) show the ω_x contours from −5f (blue) to +5f (red). f=1/T is the heaving frequency.

opening and the edge of the plate. Although for small opening ratio, stronger vortex shedding can be observed, the area of the opening is also small. With the increase of the opening ratio, the strength of the vortex decreases and the area of the opening increases, leading to the optimized opening ratio. With such opening ratio, more damping can be provided.

To investigate the effect of spacing between the plates on the flow fields, the flow fields of the double plates with different spacing are shown in Fig. 22. Around the edge of the plate, the vortical structure is basically identical. While around the edge of the opening, the vortical structure shows dependency on the spacing. For smaller spacing, as shown in Figs. 22a and 22d, the vortex generated by the opening of the upper plate has strong interaction with the jet like vortex generated by the lower plate. As shown in Figs. 22g, 22h and 22i, the size of the lower pressure region of the lower plate and the higher pressure region of the upper plate increases with the increase of spacing. Such tendency is consistent with the increase of added mass with respect to the spacing in Section 4.2. On the other hand, because of the interaction between the vortices, the jet like flow from the lower plate is weakened. As discussed previously, around the optimized opening ratio, the opening makes the main contribution to the damping of the plate. Because of such weakening, the double plates generate less averaged damping compared with the isolated plate. With the increase of spacing, the interaction between the vortex from the upper plate and the jet like vortex from the lower plate is weakened. When G/D increases to 1.00, the upper vortex interacts strongly with previous vortex, rather than the newly

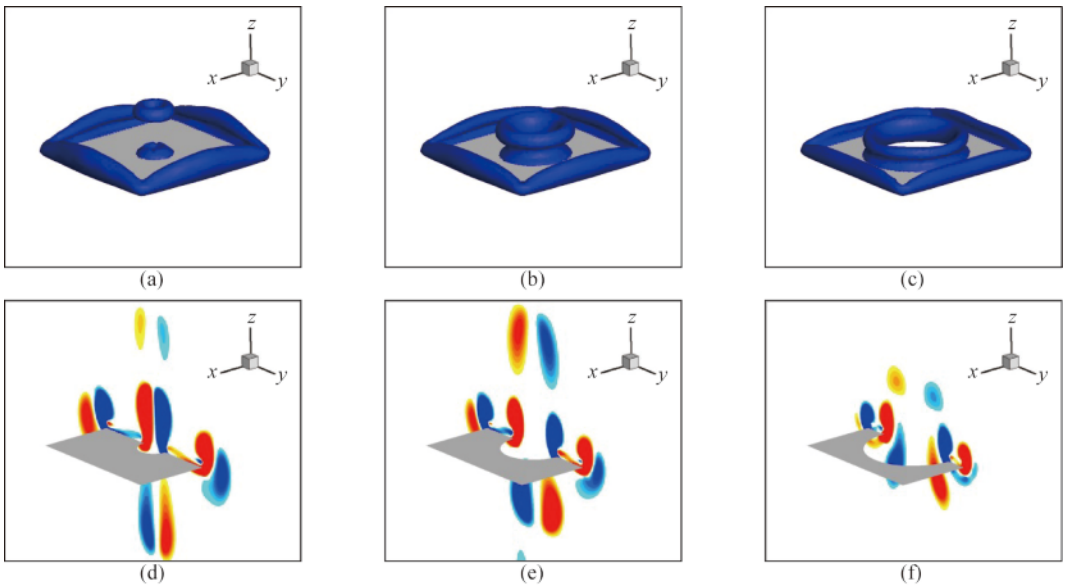

Fig. 21. Flow visualisations of the heaving plates with single circular opening. The opening ratios are 0.04 (a, d), 0.16 (b, e) and 0.36 (c, f). (a, b, c) present the 3D vortical structure around the plates identified by λ_2 criterion, where the iso-surfaces of λ_2=−50f^2 are shown. (d, e, f) show the ω_x contours from −5f (blue) to +5f (red). f=1/T is the heaving frequency.

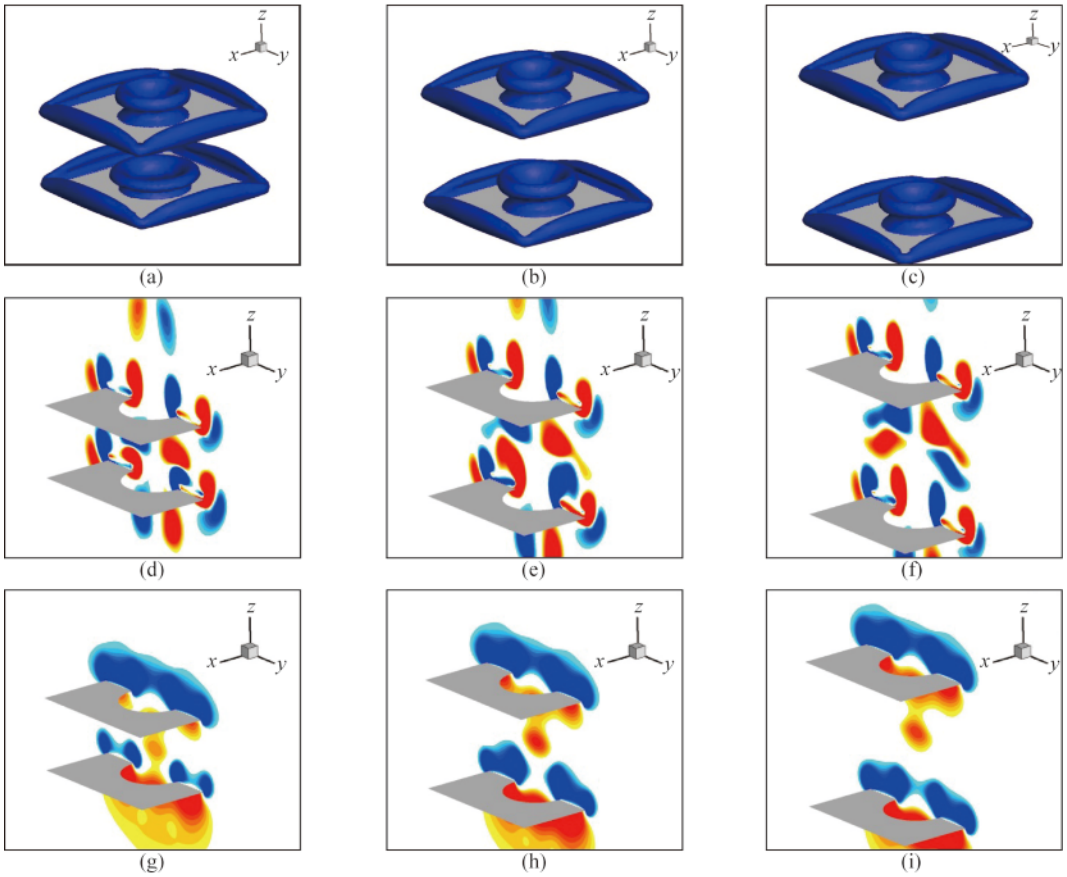

Fig. 22. Flow visualisations of double heaving plates with single circular opening and the opening ratio is 0.16. The spacing G/D is 0.50 (a, d, g), 0.75 (b, e, h) and 1.00 (c, f, i). (a, b, c) present the 3D vortical structure around the plates identified by λ_2 criterion, where the iso-surfaces of $\lambda_2=-50f^2$ are shown. (d, e, f) show the ω_x contours from $-5f$ (blue) to $+5f$ (red). $f=1/T$ is the heaving frequency. (g, h, i) show the pressure contours from $-10^{-3}\rho_0 c_s^2$ (blue) to $+10^{-3}\rho_0 c_s^2$ (red).

generated jet like vortex from the lower plate. Such interaction mode leads to larger damping compared with the case with smaller spacing.

5 Conclusions

In the current research, hydrodynamic characteristics of square heaving plates with opening under forced oscillation are investigated by an IB-LBM model. The effects of KC number, frequency number, the opening size, the opening distribution and the spacing of the plates on the hydrodynamic characteristics of the plates are examined. Here the summarized conclusions are listed briefly.

For isolated plate, the hydrodynamic characteristics show strong dependency on the opening ratio. With the increase of opening ratio, monotone decrease of the added mass can be obtained. Optimized opening ratio exists, beyond which, the damping shows monotone decrease. Compared with the opening distribution, the shape of the opening has limited effect on the hydrodynamic characteristics of the plate.

For double plates, the hydrodynamic characteristics show similar tendency about the opening ratio. As another important factor, the plate spacing also affects the hydrodynamic characteristics of the plates. With the increase of the plate spacing, both the averaged added mass and averaged damping of the double plates increase to that of the isolated plate. Optimized opening ratio also exists for double plates in the sense of damping generation.

References

Chen, S.Y. and Doolen, G.D., 1998. Lattice Boltzmann method for fluid flows, *Annual Review of Fluid Mechanics*, 30, 329–364.

Chorin, A.J., 1967. A numerical method for solving incompressible viscous flow problems, *Journal of Computational Physics*, 2(1), 12–26.

Chua, K.H., Clelland, D., Huang, S. and Sworn, A., 2005. Model experiments of hydrodynamic forces on heave plates, *Proceedings of the 24th International Conference on Offshore Mechanics and Arctic Engineering*, ASME, Halkidiki, Greece.

d'Humières, D., 2002. Multiple-relaxation-time lattice Boltzmann models in three dimensions, *Philosophical Transactions of the Royal Society A*: *Mathematical*, *Physical and Engineering Sciences*, 360(1792), 437–451.

Downie, M., Graham, J.M.R., Hall, C., Incecik, A. and Nygaard, I., 2000. An experimental investigation of motion control devices for truss spars, *Marine Structures*, 13(2), 75–90.

Feng, Z.G. and Michaelides, E.E., 2005. *Proteus*: a direct forcing method in the simulations of particulate flows, *Journal of Computa-*

tional Physics, 202(1), 20–51.

Guo, Z.L., Zheng, C.G. and Shi, B.C., 2002. Discrete lattice effects on the forcing term in the lattice Boltzmann method, *Physics Review E*, 65(4), 046308.

Holmes, S., Bhat, S., Beynet, P., Sablok, A. and Prislin, I., 2001. Heave plate design with computational fluid dynamics, *Journal of Offshore Mechanics and Arctic Engineering*, 123(1), 22–28.

Jeong, J. and Hussain, F., 1995. On the identification of a vortex, *Journal of Fluid Mechanics*, 285, 69–94.

Ji, H.T., Huang, G.L. and Fan, J., 2003. The forced oscillation tests on heave damping plates, *Journal of Shanghai Jiaotong University*, 37(7), 977–980. (in Chinese)

Lallemand, P. and Luo, L.S., 2000. Theory of the lattice Boltzmann method: dispersion. dissipation, isotropy, Galilean invariance, and stability, *Physics Review E*, 61(6), 6546–6562.

Li, J.X., Liu, S.X., Zhao, M. and Teng, B., 2013. Experimental investigation of the hydrodynamic characteristics of heave plates using forced oscillation, *Ocean Engineering*, 66, 82–91.

Patankar, S.V. and Spalding, D.B., 1972. A calculation procedure for heat. mass and momentum transfer in three-dimensional parabolic flows, *International Journal of Heat and Mass Transfer*, 15(10), 1787–1806.

Prislin, I., Blevins, R. and Halkyard, J., 1998. Viscous damping and added mass of solid square plates, *Proceedings of the 17th International Conference on Offshore Mechanics and Arctic Engineering*, ASME, Lisbon, Portugal.

Rohde, M., Kandhai, D., Derksen, J.J. and van der Akker, H.E. A., 2006. A generic. mass conservative local grid refinement technique for lattice-Boltzmann schemes, *International Journal for Numerical Methods in Fluids*, 51(4), 439–468.

Roos, F.W. and Willmarth, W.W., 1971. Some experimental results on sphere and disk drag, *AIAA Journal*, 9(2), 285–291.

Shen, W.J., Tang, Y.G. and Liu, L.Q., 2012. Research on the hydrodynamic characteristics of heave plate structure with different form edges of a spar platform, *China Ocean Engineering*, 26(1), 177–184.

Shenoy, A.R. and Kleinstreuer, C., 2008. Flow over a thin circular disk at low to moderate Reynolds numbers, *Journal of Fluid Mechanics*, 605, 253–262.

Tao, L., Molin, B., Scolan, Y.M. and Thiagarajan, K., 2007. Spacing effects on hydrodynamics of heave plates on offshore structures, *Journal of Fluids and Structures*, 23(8), 1119–1136.

Tao, L.B. and Dray, D., 2008. Hydrodynamic performance of solid and porous heave plates, *Ocean Engineering*, 35(10), 1006–1014.

Tao, L.B. and Thiagarajan, K., 2003. Low KC flow regimes of oscillating sharp edges I. Vortex shedding observation, *Applied Ocean Research*, 25(1), 21–35.

Thiagarajan, K.P. and Troesch, A.W., 1998. Effects of appendages and small currents on the hydrodynamic heave damping of TLP columns, *Journal of Offshore Mechanics and Arctic Engineering*, 120(1), 37–42.

Tian, X.L., Xiao, L.F., Zhang, X.D., Yang, J.M., Tao, L.B. and Yang, D., 2017. Flow around an oscillating circular disk at low to moderate Reynolds numbers, *Journal of Fluid Mechanics*, 812, 1119–1145.

Wu, W.W., Miao, Q.M., Kuang, X.F., Yang, L. and He, Z.M., 2009. Research on hydrodynamic characteristics of forced oscillation heave damping plates of Spar platforms, *Journal of Ship Mechanics*, 13(1), 27–33. (in Chinese)

Yang, J.M., Tian, X.L. and Li, X., 2014. Hydrodynamic characteristics of an oscillating circular disk under steady in-plane current conditions, *Ocean Engineering*, 75, 53–63.

Appendix: Convergence study

In this section, the convergence study about an isolated heaving plate with circular opening is carried out. The opening ratio is 0.16, KC=0.75 and β=200. Fig. A1 shows the time histories of the force coefficients with different grid spacing. It can be seen that the grid with h=D/80 is enough to give accurate results.

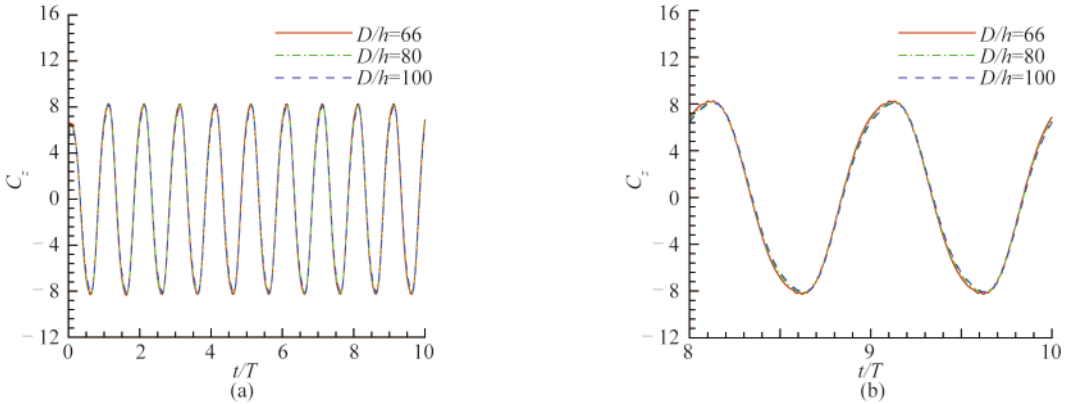

Fig. A1. Time histories of C_z with different grid spacing. The force coefficients over 10 heaving periods are shown in (a) and the detailed force coefficients over 8−10 heaving periods are shown in (b).